Macromolecules

pubs.acs.org/Macromolecules Article

Next-Generation High-Performance Biobased Naphthalate-Modified PET for Sustainable Food Packaging Applications

Ting-Han Lee, Hengzhou Liu, Michael J. Forrester, Liyang Shen, Tung-ping Wang, Huangchao Yu, Jia-Hao He, Wenzhen Li, George A. Kraus, and Eric W. Cochran*

Cite This: *Macromolecules* 2022, 55, 7785–7797 Read Online

ACCESS | Metrics & More | Article Recommendations | Supporting Information

ABSTRACT: We report a series of novel poly(ethylene terephthalate) (PET) copolymers with improved properties through the incorporation of bioadvantaged dimethyl 2,7-naphthalenedicarboxylate (2,7-N) as a comonomer. PET is among the most commonly used engineering thermoplastics, ubiquitous in the food packaging industry. However, its application is limited by poor thermal (low T_g) and oxygen barrier performance. A series of poly(ethylene terephthalate-*stat*-2,7-naphthalate) copolymers were synthesized from ethylene glycol (EG), terephthalic acid (TPA), and 2,7-N via a standard two-step melt polycondensation reaction. The 2,7-N significantly improved the thermal, mechanical, and barrier properties. The glass transition temperature (T_g > 75.4 °C) and thermal stability ($T_{d,5\%}$ > 405.1 °C) of the copolymers increase monotonically with 2,7-N content, exceeding those of PET (T_g = 69.7 °C, $T_{d,5\%}$ = 401.4 °C). Moreover, the mechanical properties and the crystallization behaviors are tunable through the 2,7-N loading. Composition-optimized copolymers showed an increase of 70% and 200% in elongation at break and tensile strength, respectively. In addition, the oxygen permeability value of the copolymers containing 20% 2,7-N loading fell to P_{O_2} = 0.0073 barrer, a 30% improvement over that of PET. These results illustrate that the novel substitution patterns offered by biobased chemicals can translate to performance advantages in packaging materials. Finally, the fundamental structure–property relationships connecting the bioadvantaged chemicals as the comonomers to the product performance were constructed as a guide for value-added renewable polymers in the future.

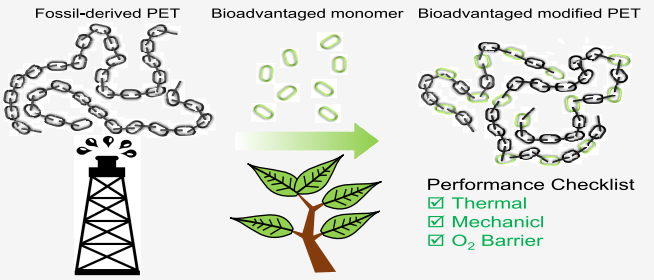

INTRODUCTION

Poly(ethylene terephthalate) (PET) is one of the most-consumed thermoplastics as well as single-use plastics (SUPs) in the world for numerous applications, representing approximately 18% of the global plastic market with an annual production of around 50 million metric tons.[1] It is a part of daily life due to its low cost, durability, and plethora of other desirable properties.[2] PET has good thermal and mechanical properties as well as excellent chemical resistance to most solvents compared to other plastics. Because of its performance, it is reported to have been used to make fibers, sheets, and films, and more specifically, it is used in food and beverage packaging, electronics and communication devices, automotive parts, lighting products, sports goods, textiles, healthcare applications, and so on.[3,4] Nonetheless, there are some shortcomings: for example, PET cannot withstand hot water cleaning and pasteurization due to its low glass transition temperature (T_g), which increases the risk for bacteria and microorganisms growth during reuse. Moreover, while the barrier performance of PET is acceptable for H_2O and CO_2, it has a poor O_2 barrier, making it poorly suited to many oxygen-sensitive products such as most liquors.[5,6]

These limitations have motivated the development of multiple pathways to improve PET performance to meet the requirements for more stringent applications. For instance, the introduction of fillers/fibers can improve the mechanical properties, although not without trade-offs.[7,8] For example, often the fillers require compatibilizers to improve interfacial adhesion, adding significant complexity and cost.[9−11] Moreover, fillers/fibers are problematic at the end of life by acting as contaminants in the recycling stream.

Alternatively, the PET resin itself can be improved upon through the partial or complete substitution of the terephthalate unit with analogous rigid segments. Comonomers like isophthalic acid (IPA), 1,4-cyclohexanedimethanol (CHDM), and diethylene glycol (DEG) are used frequently to optimize the properties for particular applications by depressing the melt temperature (e.g., for ease of processing)

Received: April 15, 2022
Revised: July 14, 2022
Published: August 24, 2022

https://doi.org/10.1021/acs.macromol.2c00777
Macromolecules 2022, 55, 7785−7797

Scheme 1. Step-Growth Polycondensation of Naphthalate-Based Copolymers via a Two-Step Polymerization

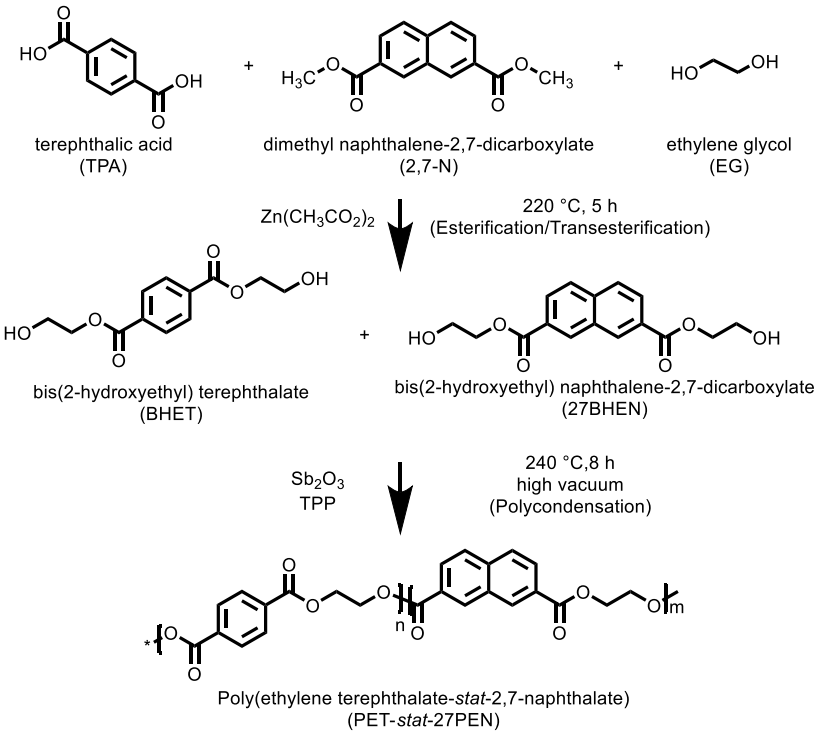

or by altering the crystallinity (e.g., for optical clarity).[12−14] Given the deterioration in some material properties, like thermal and barrier, and the petrochemical nature of these comonomers that has been questioned due to environmental concerns such as greenhouse gas emission and nonrenewable resource consumption, there is an opportunity to discover new biobased comonomers that address these issues.

Among the highest performance known terephthalate alternatives is 2,6-naphthalene dicarboxylate (2,6-N), which has received both academic and industrial attention as PET copolymers as well as in poly(ethylene 2,6-naphthalate) (26PEN) homopolymers.[15−18] The rigidity and stability of the 2,6-N fused aromatic yield polymers superior to PET in most respects including thermal, mechanical, and barrier properties. The high service temperature and barrier performance are attractive for hot-filling and liquor packaging applications; however, cost, limited availability, and environmental considerations narrow the use of 2,6-N to very high-value, low-volume applications such as high-end packaging, films, and fibers.

Given the dramatic price volatility in crude oil and concerns over the sustainability of chemical manufacturing, there is an earnest search for renewable building blocks that can compete with the petroleum-based comonomers mentioned above.[19−27] Inspired by these concerns and the potential utility of the naphthalate polyesters, we recently reported a family of biomass-derived poly(ethylene naphthalate) homopolymers as sustainable and potentially lower-cost 26PEN alternatives.[28] Among these, 2,7-naphthalene dicarboxylate (2,7-N) was found to be especially promising. Derived from malic acid, 2,7-N is structurally analogous to 2,6-N in the same manner as meta-substituted isophthalate to para-substituted terephthalate. We found that, like 26PEN, poly(ethylene 2,7-naphthalate) (27PEN) exhibits exceptional thermal and barrier performance; however, these homopolymers were brittle due to their sluggish crystallization kinetics. Thus, while 27PEN has many appealing properties, its prospects for use in applications where resilience to even modest mechanical distress appears to be limited without remediation.

The production of 2,6-N originates with the combination of *m*-xylene and butadiene and goes through a multistep process including alkylation, cyclization, (de)hydrogenation, oxidation, and so on.[29] Butadiene comes from the naphtha feedstock, which has become increasingly scarce as the refining complex has shifted to natural gas processing. It is only manufactured at select locations globally and is subject to massive price fluctuations due to crude oil. Moreover, its life cycle impacts include CO_2 emissions of 2.518 kg per kg and energy consumption of 65 MJ per kg.[30] Conversely, bioderived 2,7-N is produced primarily from malic acid, which is obtained readily from many fruit extracts, while industrial methods have focused on metabolically engineering microbial strains to generate sufficient volumes.[31] In addition, malic acid is already commercially available as a food additive for <$1 per kg in the market, which is both potentially economically and environmentally competitive compared to 2,6-N.

In a study examining the structure−property relationships in a series of nylon-6,6 copolymers, Abdolmohammadi and Gansebom et al. argued that the future of sustainable materials may be more accessible through a more gradual bootstrapping process.[32] These authors posited the view that novel "bioadvantaged" chemicals may find better value as additives that differentiate the properties of legacy materials whose support infrastructure is already in place. With respect to semicrystalline polymers like nylon-6,6, they found that up to 20 mol % of adipic acid could be replaced without severe disruptions in the nylon crystallinity that serves as the foundation for properties in that materials system. The biobased counit (*trans*-3-hexene dioate) was effectively partitioned to the amorphous phase, whose properties could

https://doi.org/10.1021/acs.macromol.2c00777
Macromolecules 2022, 55, 7785−7797

Table 1. Compositions and Characteristics of PET and Naphthalate-Based Copolymers

sample code[a]	temp/time[b] (°C/h)	IV[c] (dL/g)	M_n[d] (kDa)	M_w[e] (kDa)	$Đ$[f]	[ET]/[EN] in polymer	$L_{n,ET}$[h]	$L_{n,EN}$[h]	DR[h]
PET	240/8	0.73	16.3	27.2	1.67	100/0			
27PEN5	240/6	0.83	19.8	36.3	1.83	95.2/4.8	16.60	1.11	0.96
27PEN10	240/6	0.86	20.6	39.6	1.92	90.2/9.8	9.98	1.15	0.97
27PEN20	240/8	0.75	17.4	31.8	1.83	78.6/21.4	5.20	1.30	0.96
27PEN100[g]	240/3	0.48	11.9	42.9	3.61	0/100			

[a]Sample code: 27PEN*X*, *X* = mol % of the 2,7-N unit. [b]The esterification/transesterification reaction was performed at 220 °C for 5 h, and the bis-hydroxy ester monomer conversion of each precursor is ≥99%, which was determined by gas chromatography−mass spectrometry. [c]The intrinsic viscosity was measured in phenol/1,1,2,2-tetrachloroethane (60/40, v/v) solution by using an Ubbelohde viscometer at 25 °C. [d]Number-average molecular weight. [e]Weight-average molecular weight. [f]The dispersity was calculated by M_w/M_n. The molecular weights were determined by GPC in 1,1,1,3,3,3-hexafluoro-2-propanol solution with poly(methyl methacrylate) (PMMA) standards. [g]Poly(ethylene 2,7-naphthalate). [h]$L_{n,ET}$, $L_{n,EN}$, and DR were measured by ^{1}H NMR analysis. L_n is the average number of M1 monomer units that follow each other consecutively in a sequence uninterrupted by M2 units but bounded on each end of the sequence by M2 units. DR is a measure of the adjacency of monomers and their statistical distribution of the polymer sequence.

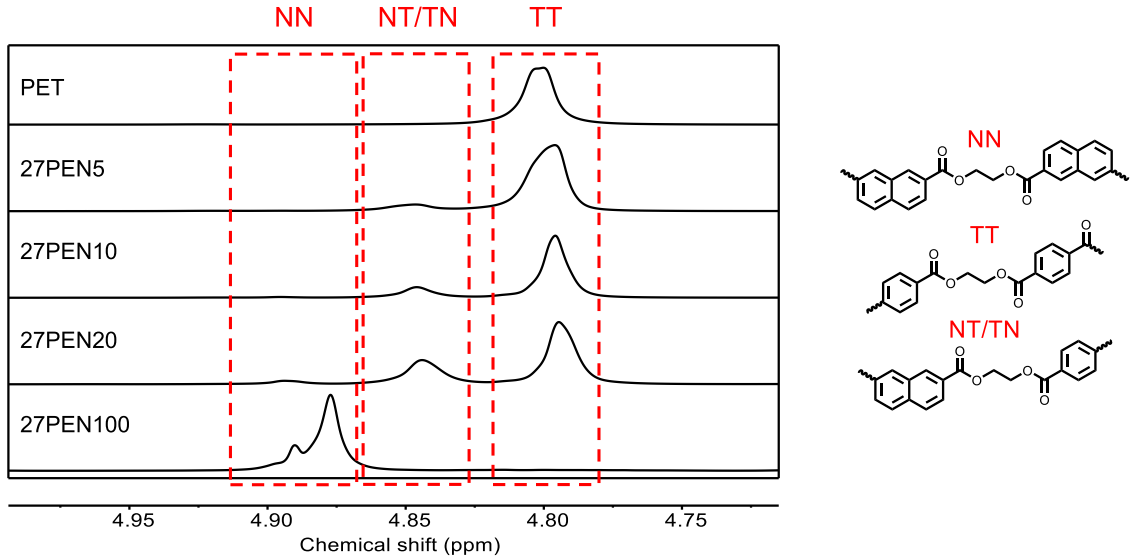

Figure 1. ^{1}H NMR spectra of the dyad fractions of NN, NT/TN, and TT of PET and naphthalate-based copolymers.

therefore be tailored somewhat independently of the crystal phase.

In this article, we hypothesized that this concept, in which the biobased counit would not significantly affect the crystallization behaviors up to a certain composition threshold and allows for the performance to be tailored, might be well-applied to realizing the potential of 2,7-N. While the sluggish 27PEN crystallization rate leads to fragile materials, its superior thermal and barrier properties could be exploited through amorphous-phase modification in PET copolymers. Success in this regard could offer a pathway for commercial adoption of 2,7-N—its role as a valorizing PET additive mitigating the costly barrier to entry associated with the immature biochemical industry. We therefore present structure−function relationships between comonomer loading and copolymer properties in a series of poly(ethylene terephthalate-*stat*-2,7-naphthalate) copolymers. These were produced by using a classic two-step melt polycondensation reaction (Scheme 1) with molecular weights similar to those of industrial-grade resins. We found that 2,7-N substitution rates near 20 mol % impart optimal improvements in thermal, mechanical, and barrier properties. These copolymers could be scalable alternatives to 26PEN/PET copolymers, providing a pathway to biochemical adoption through enabling high-value materials for demanding applications while managing product expense.

RESULTS AND DISCUSSION

We prepared a series of poly(ethylene terephthalate-*stat*-2,7-naphthalate) (27PEN*X*) copolymers as summarized in Table 1, where *X* denotes the molar 2,7-N composition. Additionally, for comparison purposes we also considered an analogous series of poly(ethylene terephthalate-*stat*-isophthalate) (PEI*X*) as described in Table S1 with *X* as the isophthalate fraction. PEI*X* and 27PEN*X* are similar in that the meta-substituted aryl content is asymmetric with respect to the chain axis in both systems; they differ due to the two fused rings of the naphthalate vs the single ring of the isophthalate. All polymers were produced by using the two-stage polymerization method and then were first characterized by using gel permeation chromatography (GPC) and intrinsic viscosity (IV) to determine the molecular weight distribution. The high $Đ$ (3.61) of 27PEN100 is likely due to mass transport limitations, which resulted from the high viscosity during polymerization compared to that of PET and 27PEN copolymers, as mentioned in our previous study.[28] The measured IV values of the polymers are consistent with the GPC results, and all polymers were within the range typical for industrially produced PET.

Beyond molecular weight, chain architecture is a critical factor in properties of copolymers. It is well-known that comonomers can have dramatically different reactivity ratios

https://doi.org/10.1021/acs.macromol.2c00777
Macromolecules 2022, 55, 7785−7797

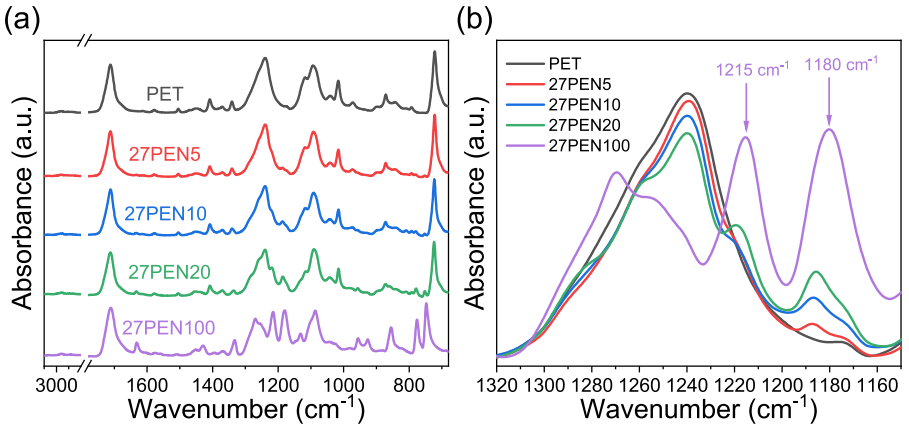

Figure 2. (a) ATR-FTIR spectra of PET and naphthalate-based copolymers and (b) the superimposed magnified spectra with wavenumbers of 1000−1400 cm^{-1}.

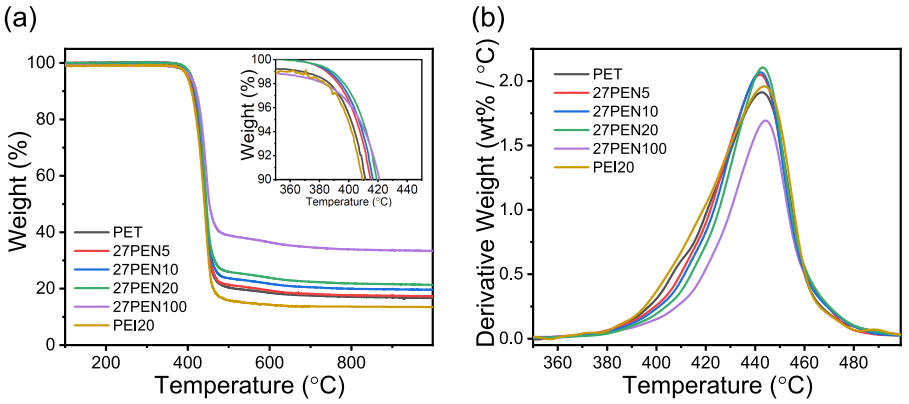

Figure 3. (a) TGA thermograms and (b) DTG curve of PET and naphthalate-based copolymers with a heating rate of 10 °C min^{-1}.

leading to heterogeneous monomer sequence distributions (MSDs). To determine the MSD, ^{1}H NMR was used to obtain information about the degree of randomness (DR), a useful heuristic in the description of copolymer microstructure. The number-average sequence lengths L_n of the ethylene terephthalate (ET) and ethylene naphthalate (EN), as well as DR, were estimated for each 27PEN*X* copolymer by using the following equations:[33]

$$L_{n,ET} = 1 + \frac{2f_{TT}}{f_{NT/TN}}, \quad L_{n,EN} = 1 + \frac{2f_{NN}}{f_{NT/TN}} \tag{1}$$

$$DR = \frac{1}{L_{n,ET}} + \frac{1}{L_{n,EN}} \tag{2}$$

where the mole fraction of each dyad sequence including f_{NN}, $f_{NT/TN}$, and f_{TT} was calculated from the integral intensities of each corresponding peak of NN, NT/TN, and TT, respectively. DR was calculated from L_{nET} and L_{nEN} values of the ET and EN units.

When the DR value is close to 1, the MSD is random, whereas the DR values of a block copolymer and alternating copolymer are 0 and 2, respectively.[34−36] ^{1}H NMR spectra of the 27PEN copolymers and peak assignments appear in Figures 1 and S1; the molar compositions of the corresponding ethylene terephthalate (ET) and ethylene naphthalate (EN) repeating units in 27PEN copolymers were estimated from these data. For the ^{1}H NMR spectrum of 27PEN20, the chemical shift of peak a (δ = 8.14 ppm) corresponds to the protons (−CH) of the single aromatic ring, whereas peak c (δ = 8.77 ppm), peak d (δ = 8.16 ppm), and peak e (δ = 7.94 ppm) represent protons (−CH) of the naphthalene ring. All 27PEN copolymers show the expected peak area which is close to the feed content of TPA and 2,7-N. The multiple peaks at 4.75−4.95 ppm are assigned to the methylene units (−CH_2−) within the ET and EN repeat units. In particular, three methylene peaks in the 27PEN20 spectrum are attributed to the four possible dyads (NN, NT/TN, TT), which can be used to estimate DR. The calculated DR values of 27PEN copolymers are close to 1, which indicated the ET and EN repeating units were randomly distributed in the copolymers.

The FTIR spectra of PET and naphthalate-based copolymers are shown in Figure 2. The strong peak at 1713 cm^{-1} is attributed to the stretching vibration of the carbonyl group (C═O) for both PET and 27PEN. The carbonyl (C−O) stretching vibration of PET appears near 1240 cm^{-1}, while that of 27PEN shifts to 1260 cm^{-1}. In particular, the peak intensity of the naphthalene ring vibration is observed at 1215 and 1180 cm^{-1} for 27PEN and the copolymers. The increase in the peak intensity of these two peaks is in accordance with the increase in the molar content of 27PEN, and there is no significant peak showing in this region for PET.

Having established the quantitative and uniform distribution of 2,7-N units in the copolymers, we next examine the thermomechanical properties as a function of composition. As a first consideration, thermal stability has to be understood (see Figure 3 and Table 4). The TGA results indicate that the thermal stability of 27PEN copolymers rises gradually with

https://doi.org/10.1021/acs.macromol.2c00777
Macromolecules 2022, 55, 7785−7797

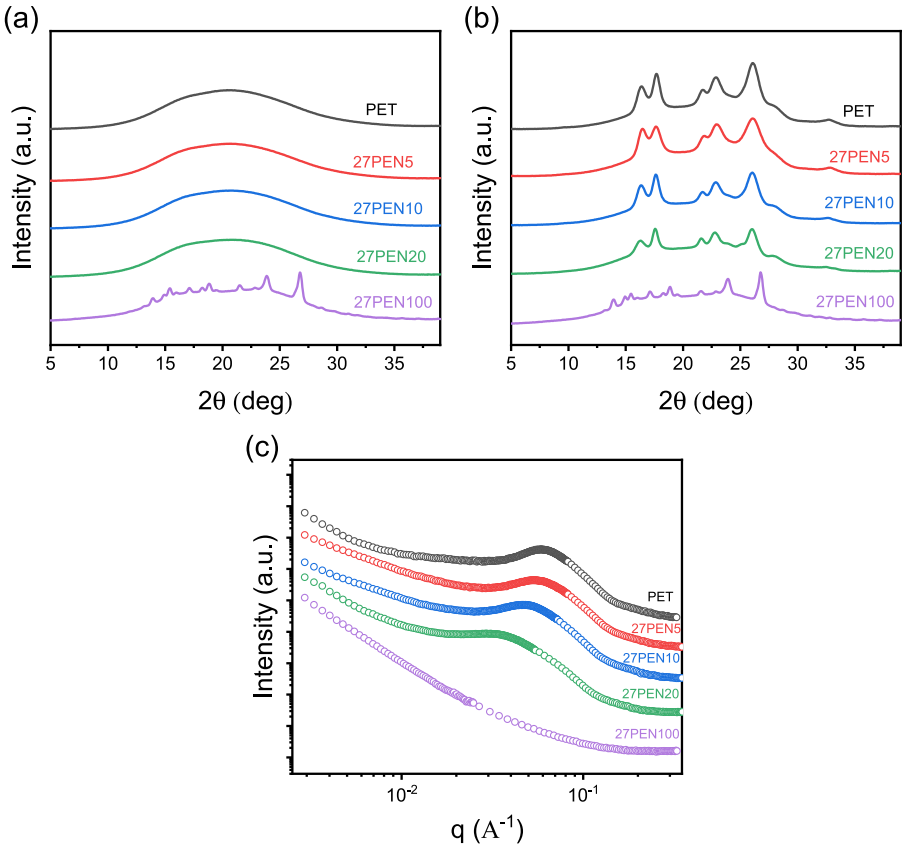

Figure 4. WAXS patterns of PET and naphthalate-based copolymers: (a) tensile bar quenched from 270 °C; (b) after annealing at 175 °C for 6 h; (c) SAXS spectra of the samples after annealing at 175 °C for 6 h.

increasing 2,7-N loading in the materials, which produce slightly more char residue and show slightly higher $T_{d,\,max}$ and $T_{d,5\%}$ values. In contrast, the thermal stability of PEI copolymers showed an opposite trend of $T_{d,\,max}$ and $T_{d,5\%}$ (see Figure S3), indicating that the thermal stability of the meta-substitution polymer (PEI) was lower than that of para-substitution polymer (PET). Therefore, the enhancement of the thermal stability was attributed to the fused aromatic rings instead of the meta-substitution orientation. Unsurprisingly, the higher % mass fraction of aromatic content in the polymer chains, the more stable the polymer will be and the higher the char residue will produce.

Because the thermal and mechanical properties are significantly dependent on the level of crystallinity and crystallization rate, DSC and WAXS were used to evaluate the effects of 2,7-N loading on the crystallization behaviors.[37−40] The WAXS/SAXS patterns of 27PEN copolymers are illustrated in Figure 4, and information regarding crystallinity is summarized in Table 2. The samples before annealing are highly amorphous, showing no WAXS diffraction peaks except 27PEN100, which has been discussed in our previous study.[28] After annealing, the 27PEN*X* diffraction peaks match those of PET homopolymer, indicating that 27PEN*X* crystals are comprised solely of PET sequences. At modest substitution rates, sequences containing 2,7-N units are too irregular to crystallize and are relegated to the amorphous phase. Furthermore, the degree of crystallinity of the copolymers decreases gradually as the content of 2,7-N increases. In the case of 27PEN copolymers, 2,7-N acts as an impurity from the viewpoint of crystallization, which disrupts the orderly fold pattern of the crystal. A similar trend is observed in PEI copolymer (see Figure S4). The rising content of IPA in the polymer chains clarifies the detrimental effect of crystallization behavior by the comonomer units.

Table 2. Crystallinity Values of PET and Naphthalate-Based Copolymers after Annealing at 175 °C for 6 h

	WAXS and SAXS				
sample code[a]	X_c (%)[b]	q_{max} (Å)	L (Å)[c]	l_c (Å)[d]	l_a (Å)[e]
PET	56.5	0.058	108.3	61.2	47.1
27PEN5	52.5	0.053	118.6	62.3	56.3
27PEN10	47.5	0.047	133.7	63.5	70.2
27PEN20	35.0	0.029	216.7	75.8	140.9
27PEN100	18.3				

[a]Sample code: 27PEN*X*, *X* = mol % of the 2,7-N unit. [b]Degree of crystallinity calculated from the WAXS pattern. [c]Lamellar thickness. [d]Crystal lamellar thickness. [e]Amorphous lamellar thickness.

Moreover, to study the effect of 2,7-N in PET chains on the lamellar periodicity of the copolymers, SAXS was performed (see Figure 4), and the results are shown in Table 2. The SAXS patterns exhibit a clear peak due to the periodic lamellar stacks, and the lamellar thickness correlates with peak position. The peak position varies monotonically as a function of 2,7-N content, as it tends to decrease as the content of fused aromatic rings rises. This implies that the long period (L, Table 2) increases along with 2,7-N loading.[41,42] The amorphous lamellar thickness (l_a) (eq 8) also increases along with 2,7-N loading, which leads to the reduction of overall crystallinity in 27PEN copolymers and is in line with the WAXS results. However, the crystal lamellar thickness (l_c) (eq 8) shows an increasing trend along with 2,7-N loading as well, which

https://doi.org/10.1021/acs.macromol.2c00777
Macromolecules 2022, 55, 7785−7797

contradicts the comonomer unit exclusion hypothesis. Hence, an alternative explanation is required. On the basis of the model proposed by previous studies, a one-dimensional correlation function, including long period (L) as well as the crystal/amorphous lamellar thickness, can be obtained by using the inverse-cosine Fourier transform of the SAXS profile.[43,44] The results imply that the crystal/amorphous lamellar thickness needs to be estimated correctly with the relative volume fraction of lamellae rather than with the bulk volume crystallinity. The results in these studies show that l_c decreases as the comonomer loading increases, in accord with the comonomer exclusion hypothesis.

The impact of 2,7-N on crystallization dynamics was also investigated through a series of isothermal DSC experiments as illustrated in Figures S5 and S6. Following Avrami kinetics, the crystallized fraction versus time follows a sigmoidal curve. The crystallization rate constant (k) increases with temperature and decreases with 2,7-N loading. The increase with temperature is due to accelerated chain mobility. The downward trend is due to the crystal disruption by 2,7-N and the higher energy requirement for chain rearrangement, which is in accordance with the WAXS results. The reciprocal crystallization half-time ($t_{1/2}^{-1}$) versus temperature is more intuitive to describe the dependence of overall crystallization rate versus temperature (Figure S7). The $t_{1/2}^{-1}$ values of 27PEN copolymers except 27PEN20 increase with temperature (faster crystallization), whereas 27PEN20 shows a downward trend. This observation can be understood through consideration of two competing factors: First, crystal nuclei are easier to form as the crystallization temperature decreases, which leads to crystallization rate acceleration. Second, the polymer chain diffusion slows down as T approaches T_g. Therefore, the crystallization rate increases as temperature is reduced when near T_m due to the increased thermodynamic driving force but passes through a maximum rate due to attenuation of the chain mobility.[45] The temperature conditions of PET and 27PEN copolymers, except 27PEN20, are dominated by the second term, whereas that of 27PEN20 is dominated by the first term.

The mechanism of nucleation and the morphology of crystal growth is suggested by the Avrami exponent n, which varies from 0.5 to 4 for most semicrystalline polymers.[46] As shown in Table 3, an average value of n = 2.5 for PET is obtained. Because PET is a pure homopolymer without any nucleating agent, the nucleation mechanism is a homogeneous nucleation followed by three-dimensional spherulite growth, in accordance with the Avrami exponent value. In contrast, the values for the copolymers are close to 2.1. This implies that 2,7-N units might act as nucleating agents because nucleation is often very sensitive to "impurities" in the system. Therefore, the crystal geometry growth of 27PEN copolymers shifts to two-dimensional axialites. As 2,7-N loading in the copolymers increases further, the development of three-dimensional order becomes more difficult and will be replaced with two-dimensional axialite. Nonetheless, because there are many other factors that would affect the nucleation of the polymer such as the free energy changes on crystallization, the lamellar thickness, and the interfacial energy, further study is required to understand the nucleation mechanism of 27PEN copolymers in future works.

The melting point T_m (see Figure 5 and Table 4) passes through a maximum in 27PEN5 and decreases thereafter, illustrating the interplay of competing enthalpic and entropic effects. At sparing 2,7-N composition, the extent of crystallinity is not yet significantly impacted; from the perspective of a crystalline PET sequence, the enthalpic penalty for melting is increased due to the thermodynamically incompatible 2,7-N units in the amorphous phase. However, at a higher 2,7-N fraction, the lamellar thickness is suppressed due to shorter PET sequences. This increases the crystallite surface area (and surface energy), depressing the melting point as anticipated by the Thompson−Gibbs equation.

Likewise, the melt recrystallization temperature T_c also passes through a maximum with respect to 2,7-N loading. On the basis of the Avrami analysis above, the comonomer unit (2,7-N) might act as a nucleation site. This tends to increase T_c as observed in 27PEN5. As the 2,7-N composition increases, however, its disruption to the regularity of crystallizable PET sequences overwhelms the nucleation effect and depresses T_c. In the case of cold crystallization, the T_{cc} trend increases along with 2,7-N loading. This could be attributed to the energy barriers for the chain motion increase with the increasing amount of fused aromatic rings, requiring greater thermal energy for chain rearrangement. A similar trend is observed in thermal behaviors of PEI copolymers (see Figure S8 and Table S2), which further demonstrates that both the comonomer units (2,7-N and IPA) can cause the disruption effect on PET crystallization ability.

In summary, the dramatic difference in the thermal properties shown between 27PEN20 and other composition copolymers can be attributed to the disruption effect of the comonomer on PET crystallization ability. When 2,7-N loading is below 10%, the crystallization ability is not yet significantly affected. However, the crystallization ability of 27PEN20 is close to the boundary that crystal formation will become critically hindered and cause the polymer to be completely amorphous. This observation is in agreement with a study exploring custom property enhancements for polyamides by bioenabled platform monomers.[47]

Turning to the amorphous phase, where the vast majority of the 2,7-N content evidently resides, all 27PEN copolymers show one unique T_g value via DSC, indicating a homogeneous

Table 3. Parameters of Isothermal Crystallization Calculated by the Avrami Equation

sample code	T_c (°C)[a]	n[a]	k[a]	$t_{1/2}$[a] (s)
PET	110	2.67	5.236×10^{-6}	82.9
	113	2.51	1.988×10^{-5}	64.5
	118	2.42	1.522×10^{-4}	32.5
	120	2.40	2.850×10^{-4}	25.8
27PEN5	125	2.23	8.994×10^{-6}	155.4
	128	2.14	2.219×10^{-5}	126.0
	130	2.21	3.800×10^{-5}	84.7
	135	2.1	1.844×10^{-4}	50.4
27PEN10	130	2.21	6.777×10^{-6}	184.9
	133	2.19	1.944×10^{-5}	119.8
	138	2.09	7.124×10^{-5}	80.9
	140	2.08	1.091×10^{-4}	67.4
27PEN20	165	2.16	6.680×10^{-7}	609.8
	170	2.24	3.404×10^{-7}	655.3
	173	2.23	2.689×10^{-7}	749.9
	175	2.28	1.584×10^{-7}	817.9

[a] T_c: the isothermal crystallization temperature; k: the crystallization rate constant; n: the Avrami exponent; $t_{1/2}$: the crystallization half-time.

https://doi.org/10.1021/acs.macromol.2c00777
Macromolecules 2022, 55, 7785−7797

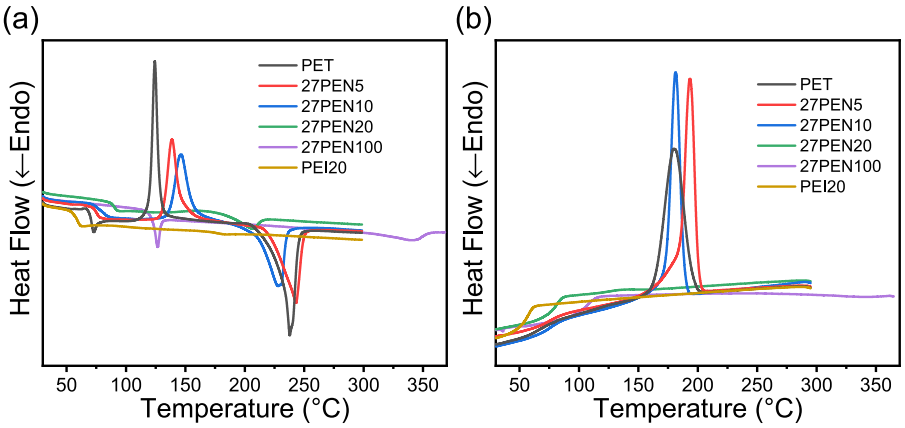

Figure 5. DSC thermograms of quenched PET and naphthalate-based copolymers at scan rate of 10 °C min^{-1}: (a) heating and (b) cooling.

Table 4. Thermal Transition Properties of PET and Naphthalate-Based Copolymers

	DSC					WAXS	TGA		
sample code[a]	T_g[b]	T_{cc}[b]	T_c[b]	T_m[b]	X_c (%)[b]	X_c (%)[c]	$T_{d,5\%}$[d]	$T_{d,max}$[d]	residue (wt %)[d]
PET	69.7	124.3	179.7	237.8	33.0	56.5	401.4	442.7	16.7
27PEN5	75.4	138.7	193.3	243.2	25.3	55.6	405.1	443.1	17.4
27PEN10	82.3	146.6	181.3	228.2	21.6	47.5	406.8	443.2	19.6
27PEN20	90.1	163.1	139.3	207.1	3.2	35.0	409.4	443.5	21.3
27PEN100	120.1	N.D.	N.D.[e]	341.0	N.A.[f]	18.3	407.3	444.3	33.4

[a]Sample code: 27PEN*X*, *X* = mol % of the 2,7-N repeat unit. [b]Glass transition (T_g), crystallization (T_c), cold crystallization (T_{cc}), and melting (T_m) temperatures, and degree of crystallinity (X_c) during the heating cycle. [c]Degree of crystallinity (X_c) after annealing at 175 °C for 6 h. [d]$T_{d,5\%}$: decomposition temperatures at which the weight loss reached 5% of its initial weight. $T_{d,max}$: the temperature at the maximum rate of decomposition. The residual mass at 1000 °C. [e]Not detected by DSC. [f]Not available.

Table 5. Mechanical and Barrier Properties of the Homo- and Copolymers

sample code[a]	Young's modulus (MPa)	yield strength (MPa)	elongation at break (%)	impact strength (J/m)	O_2 permeability (barrer)[b]
PET	1026.8 ± 23.9	73.0 ± 2.4	359.4 ± 20.1	12.6 ± 1.8	0.0108
27PEN5	1028 ± 45.5	76.1 ± 2.4	503.9 ± 46.2	13.7 ± 0.6	0.0099
27PEN10	991.1 ± 20.5	82.9 ± 5.6	611.9 ± 74.1	14.1 ± 1.8	0.0095
27PEN20	987.3 ± 19.0	77.1 ± 1.5	494.7 ± 27.8	13.1 ± 0.6	0.0073
27PEN100	756.7 ± 76.9	44.9 ± 13.0	6.5 ± 1.8	12.5 ± 1.2	0.0022
PEI10	1049.7 ± 12.2	78.2 ± 2.2	98.7 ± 18.9	12.4 ± 0.4	N.A.[c]
PEI20	1162.3 ± 95.2	78.0 ± 3.8	9.1 ± 2.0	11.9 ± 0.7	N.A.
PEI100	144.8 ± 30.7	12.3 ± 0.4	14.3 ± 2.7	9.1 ± 0.3	N.A.

[a]Sample code: 27PEN*X*/PEI*X*, *X* = mol % of the 2,7-N/IPA repeat unit. [b]1 barrer = 3.348 × 10^{-16} mol m m^{-2} s^{-1} Pa^{-1}. [c]Not available.

amorphous phase. T_g increases with 2,7-N content. 27PEN20 shows a T_g value more than 20 °C higher compared to PET, reaching T_g = 120 °C for 27PEN100. Comparison with PEI analogues shows this effect is attributed to the increased chain stiffness from the fused aromatic rings and not the meta-substitution pattern. PEI20 has a T_g about 10 °C lower than PET, dropping to 51.3 °C for PEI100 homopolymer (Figure S8 and Table S2). In conclusion, the thermal and crystallization behaviors of 27PEN copolymers can be tuned by adjusting 2,7-N content to meet the desired performance for a specific application.

In addition, to reach the target of saving cost and time as well as to predict the performance of the materials, using a model before doing experiment would be cost-effective and time-saving. The trend of T_g versus 27PEN loading shows a monotonic dependency, which can be fitted to a semiempirical equation, the Gordon−Taylor equation (eq 3), as shown in Figure S13. The higher 2,7-N loading copolymer can be estimated by using the following equation:

$$T_{g,27PENcopolymer} = \frac{k_{GT} w_1 T_{g,1} + (1 - w_1) T_{g,2}}{k_{GT} w_1 + (1 - w_1)} \quad (3)$$

where $T_{g,1}$ and $T_{g,2}$ are the glass transition temperature of 27PEN and PET homopolymer, respectively. w_1 corresponds to the weight fraction of the 27PEN units in the copolymer, and k_{GT} is the Gordon−Taylor parameter, which is an adjustable fitting parameter. A highly correlated fit was obtained with k_{GT} = 2, indicating a behavior that is typical of random copolymers.

Measuring and understanding the mechanical properties are critical for processing control as well as product development.[48] Therefore, tensile testing was used to assess the effect of 2,7-N loading in the mechanical aspect of the copolymer, as illustrated in Figure S10. It should be mentioned that the mechanical properties, especially elongation at break, can be affected by the extent of crystallinity inside PET. A small amount of crystal embedded inside the sample might result in the fracture before reaching maximum elongation at break. To

https://doi.org/10.1021/acs.macromol.2c00777
Macromolecules 2022, 55, 7785−7797

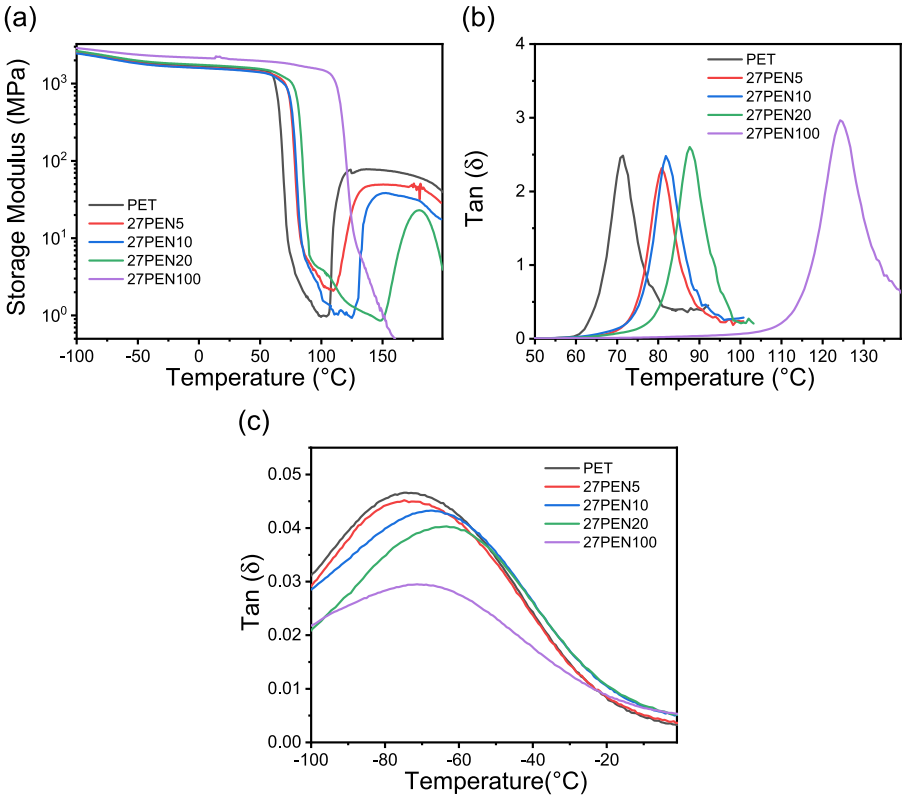

Figure 6. DMA spectra of PET and naphthalate-based copolymers: (a) storage modulus, (b) tan (δ) α-relaxation transition, and (c) tan (δ) γ-relaxation transition.

measure the true flexibility of the materials, completely amorphous tensile samples of PET and 27PEN copolymers were prepared via injection molding at 270 °C into a 40 °C mold, which was confirmed by WAXS. As shown in Table 5, 27PEN100 shows brittle performance compared to PET, which has been discussed in our previous study.[28] However, the copolymers show ductile deformation with similar yield, plastic deformation, and necking behaviors as compared to PET. Notably, PET fractures after necking with only slight strain hardening, whereas 27PEN copolymers display obvious strain hardening before breaking. Strain hardening is observed as a strengthening of a material during large strain deformation, which is attributed to the fact that the polymer chains tend to orient and align in the direction of the load and results in the crystallization of lamellar crystals perpendicular to the strain axis. The tensile strength of strain hardening shows an increase of almost 200% from 40 to 80 MPa as 2,7-N loading increases to 10% and is followed by a decrease to 70 MPa with 20% loading thereafter. This observation can be attributed to two effects: First, the increase in the rigidity of the polymer chains is due to the fused aromatic rings segment, which enables the materials to withstand higher load without being damaged. Second, the suppression effect of 2,7-N will disrupt the strain-induced crystallization, which is affirmed by the WAXS, SAXS, and DSC results. At low loading (<10%) of 2,7-N, the first term is predominant while the crystallization ability is still sufficiently high. As 2,7-N loading keeps increasing, the crystallization ability of the copolymer is dramatically affected and overwhelms the first term eventually. On the basis of the same effects mentioned above, a similar trend is also shown in elongation at break. The elongation at break shows an increase of 70% more than that of PET as 2,7-N loading increases to 10%; however, as 2,7-N loading keeps rising up to 20%, it only shows an improvement of 40% increase compared to that of PET. All the observations are in agreement with the results of PEI copolymer reported in a previous study as well as the experimental results in this work.[13]

SEM images of fractured polymer were further analyzed with the aim of providing a direct observation on the material appearance and elucidating the differences in mechanical properties, as presented in Figure S11. PET and 27PEN*X* copolymers exhibited a massive network of cracks across the specimen surface, indicating the ability of these materials to dissipate energy throughout the sample. In contrast, 27PEN100 shows a smooth surface with tiny crystals, which has been discussed in a previous study.[28] Analysis of surface appearance confirmed that 27PEN*X* copolymers possess a similar energy dissipating ability to that of PET.

In addition to thermal, crystallization, and mechanical aspects, barrier performance is also critical for making useful single-use packaging equipment. To that end, the effect of PET modification by 2,7-N on the barrier properties must be studied to meet Food and Drug Administration requirements for food packaging. Herein, the γ-relaxation could be expressed by a change in activation energy for either diffusion or permeation which relates to barrier properties; thus, DMA was performed to investigate low-temperature molecular motions of 27PEN copolymers (see Figure 6c).[49−52] As 2,7-N loading in the polymer chain increased, the T_γ transition increased from −74.2 to −63.4 °C, indicating that more energy is needed for the copolymer to carry out localized chain motion. Furthermore, it appears that the observed reduction in γ-relaxation peak areas is entirely the result of modifying PET polymer chain with a meta-substitution fused aromatic ring,

https://doi.org/10.1021/acs.macromol.2c00777
Macromolecules 2022, 55, 7785−7797

which restricted sub-T_g molecular motions. The observation for this change can be separated into two effects: First is the incorporation of the restricted mobility naphthalene ring in the polymer chains, which is in accordance with the trend reported in the literature.[53] Second, the meta-substitution structure decreases the chain mobility compared to the para-substitution structure. A similar trend shown in PEI copolymers (see Figure S12) further illustrated that the meta-structure repeating unit could suppress the ring flip motion of the para-structure polymer.

In addition to the γ-transition, the α-transition and crystallization behaviors of 27PEN copolymers were studied. The peak of the α-transition (denoted as T_α in Figure 6) increases with the increasing amount of 2,7-N. This is attributed to the inhibition of the free movement of the polymer chain in amorphous phase from the embedded fused aromatic rings segment. The T_α value is comparable to the T_g determined by DSC, which indicates that the copolymer with higher 2,7-N loading possesses a higher service temperature. The subsequent increase in storage modulus (related to the elasticity of the material) after the α-transition reached the rubbery plateau was attributed to cold crystallization, which was associated with the density modulation caused by the formation of a crystalline phase.[54] The starting temperature of cold crystallization increases along with 2,7-N loading in the copolymers, which further proves the interference effect of 2,7-N on crystallization, consistent with the cold crystallization results detected by DSC. It should be noted that the value of storage modulus decreases progressively with 2,7-N loading. It is probable that the reduced crystal packing efficiency afforded by comonomer loading largely depresses the crystal lamellar thickness and causes the elasticity to drop. This phenomenon becomes more pronounced with increased 2,7-N loading, and the rubbery plateau related to cold crystallization will vanish when the crystallization ability is completely destroyed.

These cooperative relaxation phenomena are implicitly related to the gas permeability. The oxygen barrier performance is very important to many performance packaging applications. As shown in Table 5, the oxygen permeability of 27PEN copolymers decreases monotonically with 2,7-N loading. The oxygen barrier performance of 27PEN20 (0.0073 barrer) shows a 30% improvement over PET (0.0108 barrer) with only 20% 2,7-N embedded in PET chains, indicating the barrier capability of meta-substitution fused aromatic rings is 2 times better than that of commercial used para-substitution fused aromatic rings (26NDA) reported in the previous study.[55] This is mainly attributable to restricted ring flip associated with the nonlinear axis of meta-naphthalene structure, which would suppress the chain rotation and mobility related directly to gas diffusivity.

In summary, 27PEN copolymers showed improved performance compared to PET with respect to thermal, mechanical, and barrier properties, which strongly suggests that these copolymers with value-added property improvement using biosourced 2,7-N are promising candidate materials for broader packaging applications. Nonetheless, more analyses, including techno-economic assessment, life-cycle assessment, and toxicological evaluations of 2,7-N, would be would be necessary before being commercialized in large scale for food packaging.

CONCLUSIONS

In this work, PET incorporated with bioderived naphthalate-based monomers were successfully synthesized by a two-step melt polycondensation reaction. ^{1}H NMR analysis revealed that the synthesized copolymers were statistically random copolymers, and the molar ratio of 2,7-N in the copolymers was consistent with that of the input reactants. Comonomer units were found to partition into the amorphous phase while leaving the crystal lattice units unaltered. 2,7-N acted as an impurity from the viewpoint of crystallization, which significantly affected the nucleation mechanism and crystallization ability of the materials. The observed results were the change in crystal geometry from 3D spherulite growth to 2D axialite growth as well as the increasing suppression effect on crystal lamellar thickness with increasing 2,7-N loading. The effect that 2,7-N imposed on crystallization behaviors was the key to the improvement of thermal and mechanical properties. By analysis using various methods, it was confirmed that 2,7-N has a positive effect on the drawbacks of PET, where 27PEN10 in particular showed a dramatic increase in all the properties while retaining most of the crystallization behaviors of PET. The T_g of 27PEN10 is 15 °C higher than that of PET, which is due to the increased energy barrier of the chain motion for the polymer chains in amorphous domain, whereas the increased rigidity of the polymer chain caused by fused aromatic rings resulted in the improvement in strain hardening and elongation at break. Moreover, the restricted ring flip associated with the nonlinear axis of meta-naphthalene structure effectively suppressed the oxygen permeability of the materials. These results suggest that bioadvantaged comonomers like 2,7-N are capable of being used for modifying polymer properties, in both sustainability and performance compared with those of traditional PET. The strategy in this work would not only allow PET to have widespread applications requiring higher service temperature, and better barrier/mechanical properties, but also constructed the fundamental structure−property relationships connecting the bioadvantaged chemicals as hard segment inside polymers to its performance. Compared to the petroleum-derived chemicals (IPA, CHDM, DEG) which are widely available and under commercial development including techno-economic model development, 2,7-N is a potential bioderived chemical, which could be used in PET property enhancements, and further studies like techno-economic and life-cycle assessment would be needed to be developed. In general, by utilizing bioadvantaged monomers, the economic incentive for adoption and industry growth of biochemicals can be provided, and capital requirements for product startup can be simultaneously minimized.

EXPERIMENTAL SECTION

Materials. Terephthalic acid (TPA, 99+%, Acros Organics), isophthalic acid (IPA, 99+%, TCI America), and ethylene glycol (EG, anhydrous, 99.8%, Sigma-Aldrich) were purchased as the precursors for polymer synthesis. Dimethyl naphthalene-2,7-dicarboxylate (2,7-N) was synthesized based on the reaction procedures reported in our previous study.[28] Zinc acetate ($Zn(CH_3COO)_2$), anhydrous, 99.8%, Alfa Aesar) and antimony(III) oxide (Sb_2O_3, 99%, Sigma-Aldrich) were used as catalysts in transesterification and polycondensation reaction, respectively. Triphenyl phosphate (TPP, >99%, Sigma-Aldrich) was used as a thermal stabilizer in polycondensation reaction. 1,1,1,3,3,3-Hexafluoro-2-propanol (HFIP), dichloroacetic acid (DCAA), phenol, 1,1,2,2-tetrachloroethane, trifluoroacetic acid-*d* (TFA-*d*), and chloroform-*d* ($CDCl_3$)

https://doi.org/10.1021/acs.macromol.2c00777
Macromolecules 2022, 55, 7785−7797

were purchased from Fisher Scientific and were used as received for solvent and sample preparation.

Synthesis. The homo- and copolymers were synthesized by using a 300 mL stainless steel reactor (type 4560, Parr Instrument Company) equipped with mechanical stirrers, reactor controller (model 4848, Parr Instrument Company), liquid nitrogen cold traps, and a vacuum pump (DUO 10, Pfeiffer Vacuum). Poly(ethylene terephthalate-*stat*-2,7-naphthalate) (27PENX) and poly(ethylene terephthalate-*stat*-isophthalate) (PEIX) were synthesized by a two-step polycondensation reaction (see Schemes 1 and S1). The first step was esterification as well as transesterification of TPA/2,7-N or TPA/IPA with EG, respectively, using $Zn(CH_3COO)_2$ (0.15 mol % to diester) as the transesterification catalyst. For TPA/IPA esterification, no catalyst is needed since diacid served as both reagent and catalyst.[56] The molar ratio of overall diacid/diester to EG was 1 to 10. The purpose of this molar ratio is to prepare completely bis-hydroxy ester end group monomers and ensure both end groups have the same reactivity toward other monomers. This will make the growth of polymer chain more consistent and lower the dispersity compared to the different end group monomers. The reaction mixture was purged with argon for 0.5 h, and the reaction temperature was heated to 220 °C. The stirring speed was set at 250 rpm for 5 h with the pressure at 110 psi and an argon sweep to remove water and methanol. After the first step reaction, the mixture was transferred to a round-bottom flask to distill the excess amount of EG by using an oil bath set to 110 °C under vacuum for 12 h. Then the monomer was returned to the autoclave reactor with antimony(III) oxide (0.02 mol % to the diacid/diester) and triphenyl phosphate (0.1 mol % to the diacid/diester) acting as catalyst and thermal stabilizer, respectively. The second step of polycondensation was performed at 240 °C under high vacuum with the stirring speed at 600 rpm. At the end of the reaction, the reactor was purged by argon to ambient pressure to prevent thermal oxidation of the material while removing the polymer from the reactor.

Characterization. The composition and the chemical structures were determined by ^{1}H NMR (600 MHz, Bruker Avance III) in a $CDCl_3$/TFA-*d* (75/25) solvent mixture at 10 mg/mL.

The molar composition of the copolymers was calculated based on the integral intensities of peak a from PET units and peak c from 27PEN units by using the following equation:

$$\mathrm{ET} = \frac{\frac{I_a}{4}}{\frac{I_a}{4} + \frac{I_c}{2}}, \quad \mathrm{EN} = \frac{\frac{I_c}{2}}{\frac{I_a}{4} + \frac{I_c}{2}} \tag{4}$$

where the contents of ET and EN unit were their molar ratio in the polymer chain and I_a and I_c correspond to the protons on the aromatic ring of ET and EN, respectively.

The intrinsic viscosity $[\eta]$ measurement was performed in a phenol/1,1,2,2-tetrachloroethane (60/40, v/v) solvent mixture at 25 °C water bath by using an Ubbelohde viscometer (Xylem, type 537 13).

Gel permeation chromatography (GPC) measurements were running at a flow rate of 0.3 mL/min in a Tosoh Ecosec GPC (Tosoh Ecosec HLC-8320GPC) equipped with UV and RI detectors. The concentration of samples was 6 mg/mL in the HFIP/DCAA (50/50, v/v) solvent mixture, and HFIP was used as an eluent. Poly(methyl methacrylate) (PMMA) standards were used to determine the molecular weights.

FTIR (iD7 ATR accessory for the Nicolet iS 5 spectrometer, ThermoFisher) was used to analyze functionality. Spectra were obtained from 4000 to 400 cm^{-1} from 32 scans at a resolution of 4 cm^{-1}.

The crystal structure morphology and the extent of crystallinity were characterized by a Xenocs Xeuss 2.0 S/WAXS system equipped with a Cu Kα X-ray source. The data were collected by a Dectris Pilatus3 R 1M detector and was calibrated by the silver behenate standard. The specimens were attached directly onto the sample stage, and the measurement was performed under vacuum. Data acquisitions for WAXS and SAXS analysis were 600 and 7200 s, respectively. The background signal of each samples was taken at the same condition. All data postprocessing was performed by using Foxtrot 3.3.4 (SOLEIL Synchrotron, France) for 2D raw data reduction and absolute intensity correction and the Irena package (Advanced Photon Source, Argonne National Lab, USA) for profile combination.[57] The crystal structure information was calculated by using scattering vector (eqs 5 and 6).

$$q = \frac{4\pi}{\lambda} \sin\theta \tag{5}$$

$$L = \frac{2\pi}{q_{\max}} \tag{6}$$

$$X_c = \frac{A_c}{A_a + A_c} \times 100\% \tag{7}$$

where λ is the X-ray wavelength for Cu Kα radiation (λ = 1.542 Å), θ is Bragg's angle, and q_{max} is peak position in the q range. The degree of crystallinity (X_c) was measured by eq 7 based on the ratio of the crystalline fraction (A_c) to the total area ($A_a + A_c$) under the WAXS curve.

The crystalline lamellar thickness (l_c) and amorphous lamellar thickness (l_a) in the lamellar stacks can be estimated from the WAXS and SAXS results via eq 8, where the amorphous region is assumed to be located only within the lamellar stacks.

$$l_c = LX_c, \quad l_a = LX_a \tag{8}$$

Thermal characterizations were conducted by using differential scanning calorimetry (DSC, TA Instruments Q2500) under nitrogen. The specimens from injection molding were conducted from 25 to 300 °C (27PEN100 to 370 °C) at a rate of 10 °C min^{-1} and were held for 5 min before being cooled back to 25 °C at a rate of 10 °C min^{-1}. The isothermal crystallization kinetics were performed on completely amorphous tensile bar samples in the temperature range from 110 to 175 °C. Samples were placed in DSC at 25 °C and heated to the desired temperature at 160 °C min^{-1}. They were kept at the crystallization temperature for a sufficient period until the completion of crystallization. Thermal stability was evaluated by a simultaneous thermal analyzer (STA 449 F1 Jupiter, NETZSCH) in the temperature range from 40 to 1000 °C at a rate of 10 °C min^{-1} under nitrogen.

Tensile tests were performed by an Instron 3369 at room temperature with a 1 kN load cell and a speed of 10 mm min^{-1} following the standards of ISO 527-2. The dimension of the tensile bar is type 1BB with 2 mm (thickness) × 10 mm (guage length). The impact strength of the samples were conducted by an impact tester (IT504, Tinius Olsen) according to the standards of ASTM D256 with the sample dimension of 63.5 mm (length) × 12.7 mm (width) × 3 mm (thickness).

The cryofractured surface were photographed by a scanning electron microscope (S4800 FE-SEM, Hitachi) at 10 kV SEM acceleration voltage. The samples from injection molding were frozen in liquid nitrogen for 5 min before being fractured.

The dynamic mechanical measurements were performed on a rheometer (ARES-G2, TA Instruments) using the torsion fixture at a constant frequency of 1 Hz and a strain of 0.1%. The testing was conducted from −120 to 200 °C at a heating rate of 5 °C min^{-1}.

The gas barrier property was measured by an oxygen permeation testing analyzer (MOCON's OX-TRAN model 2/21) under a carrier gas mixture of 98% nitrogen and 2% hydrogen and a test gas of 99.9% oxygen. The analysis procedure is based on ASTM D3985 standards. The specimens with 0.5 mm thickness were prepared via injection molding (HAAKE Minijet, ThermoFisher) at 270 °C into a 120 °C mold and quenched in cold water bath. The permeability of the films was measured via oxygen transmission at 23 °C under 1% relative humidity and 1 atm.[58,59]

https://doi.org/10.1021/acs.macromol.2c00777
Macromolecules 2022, 55, 7785−7797

■ ASSOCIATED CONTENT

Supporting Information

The Supporting Information is available free of charge at https://pubs.acs.org/doi/10.1021/acs.macromol.2c00777.

Additional experimental details, including isothermal crystallization kinetics study, isophthalate-based copolymer synthesis pathway and its characterization, GPC analysis, SEM images, and mechanical tensile testing (PDF)

■ AUTHOR INFORMATION

Corresponding Author

Eric W. Cochran − *Department of Chemical and Biological Engineering, Iowa State University, Ames, Iowa 50011, United States;* orcid.org/0000-0003-3931-9169; Email: ecochran@iastate.edu

Authors

Ting-Han Lee − *Department of Chemical and Biological Engineering, Iowa State University, Ames, Iowa 50011, United States;* orcid.org/0000-0002-5531-052X

Hengzhou Liu − *Department of Chemical and Biological Engineering, Iowa State University, Ames, Iowa 50011, United States*

Michael J. Forrester − *Department of Chemical and Biological Engineering, Iowa State University, Ames, Iowa 50011, United States;* orcid.org/0000-0003-3063-9975

Liyang Shen − *Department of Chemical and Biological Engineering, Iowa State University, Ames, Iowa 50011, United States;* orcid.org/0000-0001-9928-2877

Tung-ping Wang − *Department of Chemical and Biological Engineering, Iowa State University, Ames, Iowa 50011, United States;* orcid.org/0000-0001-6292-3933

Huangchao Yu − *Department of Chemistry, Iowa State University, Ames, Iowa 50011, United States*

Jia-Hao He − *Department of Agricultural and Biosystems Engineering, Iowa State University, Ames, Iowa 50011, United States;* orcid.org/0000-0001-7596-9156

Wenzhen Li − *Department of Chemical and Biological Engineering, Iowa State University, Ames, Iowa 50011, United States;* orcid.org/0000-0002-1020-5187

George A. Kraus − *Department of Chemistry, Iowa State University, Ames, Iowa 50011, United States;* orcid.org/0000-0002-3037-8413

Complete contact information is available at: https://pubs.acs.org/10.1021/acs.macromol.2c00777

Notes

The authors declare no competing financial interest.

■ ACKNOWLEDGMENTS

The authors thank Lucas Showman at W. M. Keck Metabolomics Research Laboratory for the assistance on Agilent GC-MS and Sarah Cady at ISU Chemical Instrumentation Facility (CIF) for the assistance on the Bruker 600 MHz NMR. Finally, we acknowledge financial support from the Center for Bioplastics and Biocomposites and DMR-1626315.

■ REFERENCES

(1) Eerhart, A.; Faaij, A.; Patel, M. Replacing fossil based PET with biobased PEF; process analysis, energy and GHG balance. *Energy Environ. Sci.* **2012**, *5*, 6407−6422.

(2) Sinha, V.; Patel, M. R.; Patel, J. V. PET waste management by chemical recycling: a review. *Journal of Polymers and the Environment* **2010**, *18*, 8−25.

(3) Shojaei, B.; Abtahi, M.; Najafi, M. Chemical recycling of PET: A stepping-stone toward sustainability. *Polym. Adv. Technol.* **2020**, *31*, 2912−2938.

(4) Yue, Q.; Wang, C.; Zhang, L.; Ni, Y.; Jin, Y. Glycolysis of poly (ethylene terephthalate)(PET) using basic ionic liquids as catalysts. *Polym. Degrad. Stab.* **2011**, *96*, 399−403.

(5) Polyakova, A.; Liu, R.; Schiraldi, D.; Hiltner, A.; Baer, E. Oxygen-barrier properties of copolymers based on ethylene terephthalate. *J. Polym. Sci., Part B: Polym. Phys.* **2001**, *39*, 1889−1899.

(6) Cava, D.; Giménez, E.; Gavara, R.; Lagaron, J. Comparative performance and barrier properties of biodegradable thermoplastics and nanobiocomposites versus PET for food packaging applications. *Journal of Plastic Film & Sheeting* **2006**, *22*, 265−274.

(7) Shen, L.; Wang, T.-p.; Lin, F.-Y.; Torres, S.; Robison, T.; Kalluru, S. H.; Hernández, N. B.; Cochran, E. W. Polystyrene-*block*-Polydimethylsiloxane as a potential silica substitute for polysiloxane reinforcement. *ACS Macro Lett.* **2020**, *9*, 781−787.

(8) Shen, L.; Wang, T.-p.; Goyal, S.; Lee, T.-H.; Lin, F.-Y.; Torres, S.; Robison, T.; Cochran, E. W. Easy-Processable and Aging-Free All-Polymer Polysiloxane Composites. *ACS Appl. Polym. Mater.* **2020**, *2*, 5835−5844.

(9) López de Dicastillo, C.; Velásquez, E.; Rojas, A.; Guarda, A.; Galotto, M. J. The use of nanoadditives within recycled polymers for food packaging: Properties, recyclability, and safety. *Comprehensive Reviews in Food Science and Food Safety* **2020**, *19*, 1760−1776.

(10) Rezaeian, I.; Jafari, S.; Zahedi, P.; Nouri, S. An investigation on the rheology, morphology, thermal and mechanical properties of recycled poly (ethylene terephthalate) reinforced with modified short glass fibers. *Polym. Compos.* **2009**, *30*, 993−999.

(11) Khan, M. Z.; Srivastava, S. K.; Gupta, M. Tensile and flexural properties of natural fiber reinforced polymer composites: A review. *Journal of Reinforced Plastics and Composites* **2018**, *37*, 1435−1455.

(12) Hergenrother, W. Influence of copolymeric poly (diethylene glycol) terephthalate on the thermal stability of poly (ethylene terephthalate). *J. Polym. Sci.: Polym. Chem. Ed.* **1974**, *12*, 875−883.

(13) Karayannidis, G. P.; Sideridou, I. D.; Zamboulis, D. N.; Bikiaris, D. N.; Sakalis, A. J. Thermal behavior and tensile properties of poly (ethylene terephthalate-co-ethylene isophthalate). *J. Appl. Polym. Sci.* **2000**, *78*, 200−207.

(14) Chen, T.; Zhang, W.; Zhang, J. Alkali resistance of poly (ethylene terephthalate)(PET) and poly (ethylene glycol-co-1, 4-cyclohexanedimethanol terephthalate)(PETG) copolyesters: The role of composition. *Polym. Degrad. Stab.* **2015**, *120*, 232−243.

(15) Ihm, D. W.; Park, S. Y.; Chang, C. G.; Kim, Y. S.; Lee, H. K. Miscibility of poly (ethylene terephthalate)/poly (ethylene 2, 6-naphthalate) blends by transesterification. *J. Polym. Sci., Part A: Polym. Chem.* **1996**, *34*, 2841−2850.

(16) Lee, S. C.; Yoon, K. H.; Park, I. H.; Kim, H. C.; Son, T. W. Phase behaviour and transesterification in poly (ethylene 2, 6-naphthalate) and poly (ethylene terephthalate) blends. *Polymer* **1997**, *38*, 4831−4835.

(17) Aoki, Y.; Li, L.; Amari, T.; Nishimura, K.; Arashiro, Y. Dynamic mechanical properties of poly (ethylene terephthalate)/poly (ethylene 2, 6-naphthalate) blends. *Macromolecules* **1999**, *32*, 1923−1929.

(18) Chen, C.-W.; Yang, Y.-H.; Lin, S.-C.; Rwei, S.-P.; Shyr, T.-W. Crystal Structure and Tensile Fracture Morphology of Poly (ethylene terephthalate)-co-poly (ethylene 2, 6-naphthalate) Block Copolyesters and Fibers. *Ind. Eng. Chem. Res.* **2020**, *59*, 18717−18725.

(19) Zhang, Y. The Links between the Price of Oil and the Value of US Dollar. *International Journal of Energy Economics and Policy* **2013**, *3*, 341−351.

(20) Lipinsky, E. Chemicals from biomass: petrochemical substitution options. *Science* **1981**, *212*, 1465−1471.

(21) Liu, H.; Lee, T.-H.; Chen, Y.; Cochran, E.; Li, W. Paired and Tandem Electrochemical Conversion of 5-(Hydroxymethyl) furfural

Using Membrane-Electrode Assembly-Based Electrolytic Systems. *ChemElectroChem.* **2021**, *8*, 2817−2824.
(22) Liu, H.; Lee, T.-H.; Chen, Y.; Cochran, E. W.; Li, W. Paired electrolysis of 5-(hydroxymethyl) furfural in flow cells with a high-performance oxide-derived silver cathode. *Green Chem.* **2021**, *23*, 5056−5063.
(23) Goyal, S.; Lin, F.-Y.; Forrester, M.; Henrichsen, W.; Murphy, G.; Shen, L.; Wang, T.-p.; Cochran, E. W. Glycerol Ketals as Building Blocks for a New Class of Biobased (Meth) acrylate Polymers. *ACS Sustainable Chem. Eng.* **2021**, *9*, 10620−10629.
(24) Forrester, M.; Becker, A.; Hohmann, A.; Hernandez, N.; Lin, F.-Y.; Bloome, N.; Johnson, G.; Dietrich, H.; Marcinko, J.; Williams, R. C.; et al. RAFT thermoplastics from glycerol: a biopolymer for development of sustainable wood adhesives. *Green Chem.* **2020**, *22*, 6148−6156.
(25) Lin, F.-Y.; Hohmann, A. D.; Hernández, N.; Shen, L.; Dietrich, H.; Cochran, E. W. Self-Assembly of Poly (styrene-*block*-acrylated epoxidized soybean oil) Star-Brush-Like Block Copolymers. *Macromolecules* **2020**, *53*, 8095−8107.
(26) Lin, F.-Y.; Yan, M.; Cochran, E. W. Gelation Suppression in RAFT Polymerization. *Macromolecules* **2019**, *52*, 7005−7015.
(27) Carraher, J. M.; Carter, P.; Rao, R. G.; Forrester, M. J.; Pfennig, T.; Shanks, B. H.; Cochran, E. W.; Tessonnier, J.-P. Solvent-driven isomerization of cis, cis-muconic acid for the production of specialty and performance-advantaged cyclic biobased monomers. *Green Chem.* **2020**, *22*, 6444−6454.
(28) Lee, T.-H.; Yu, H.; Forrester, M.; Wang, T.-p.; Shen, L.; Liu, H.; Li, J.; Li, W.; Kraus, G.; Cochran, E. Next-Generation High-Performance Bio-Based Naphthalate Polymers Derived from Malic Acid for Sustainable Food Packaging. *ACS Sustainable Chem. Eng.* **2022**, *10*, 2624−2633.
(29) Scheirs, J.; Long, T. E. *Modern Polyesters: Chemistry and Technology of Polyesters and Copolyesters*; John Wiley & Sons: 2005.
(30) Cabrera Camacho, C.; Alonso-Farinas, B.; Villanueva Perales, A.; Vidal-Barrero, F.; Ollero, P. Techno-economic and life-cycle assessment of one-step production of 1, 3-butadiene from bioethanol using reaction data under industrial operating conditions. *ACS Sustainable Chem. Eng.* **2020**, *8*, 10201−10211.
(31) Lee, J. J.; Pollock, G. R., III; Mitchell, D.; Kasuga, L.; Kraus, G. A. Upgrading malic acid to bio-based benzoates via a Diels−Alder-initiated sequence with the methyl coumalate platform. *RSC Adv.* **2014**, *4*, 45657−45664.
(32) Abdolmohammadi, S.; Gansebom, D.; Goyal, S.; Lee, T.-H.; Kuehl, B.; Forrester, M. J.; Lin, F.-Y.; Hernández, N.; Shanks, B. H.; Tessonnier, J.-P.; et al. Analysis of the Amorphous and Interphase Influence of Comononomer Loading on Polymer Properties toward Forwarding Bioadvantaged Copolyamides. *Macromolecules* **2021**, *54*, 7910−7924.
(33) Paek, K. H.; Im, S. G. Synthesis of a series of biodegradable poly (butylene carbonate-co-isophthalate) random copolymers derived from CO 2-based comonomers for sustainable packaging. *Green Chem.* **2020**, *22*, 4570−4580.
(34) Zhu, W.; Zhou, W.; Li, C.; Xiao, Y.; Zhang, D.; Guan, G.; Wang, D. Synthesis, characterization and degradation of novel biodegradable poly (butylene-co-hexamethylene carbonate) copoly-carbonates. *Journal of Macromolecular Science, Part A* **2011**, *48*, 583−594.
(35) Japu, C.; Martinez de Ilarduya, A.; Alla, A.; Garcia-Martin, M. G.; Galbis, J. A.; Munoz-Guerra, S. d-Glucose-derived PET copolyesters with enhanced Tg. *Polym. Chem.* **2013**, *4*, 3524−3536.
(36) Han, J.; Shi, J.; Xie, Z.; Xu, J.; Guo, B. Synthesis, properties of biodegradable poly (butylene succinate-co-butylene 2-methylsuccinate) and application for sustainable release. *Materials* **2019**, *12*, 1507.
(37) Deshpande, V.; Jape, S. Isothermal crystallization kinetics of anhydrous sodium acetate nucleated poly (ethylene terephthalate). *J. Appl. Polym. Sci.* **2010**, *116*, 3541−3554.
(38) Xing, S.; Tang, P.; Yang, Y. Poly (styrene-co-maleic anhydride) ionomers as nucleating agent on the crystallization behavior of poly (ethylene terephthalate). *J. Appl. Polym. Sci.* **2015**.
(39) Liu, H.; Ma, J.; Zhu, C.; Xu, J.; Gong, J. Miscibility and crystallization behavior of poly (ethylene terephthalate)/phosphate glass hybrids. *Journal of Macromolecular Science, Part B* **2016**, *55*, 1039−1050.
(40) Kim, K.; Rahimi, S. K.; Alam, T. M.; Sorte, E. G.; Otaigbe, J. U. Unexpected effects of inorganic phosphate glass on crystallization and thermo-rheological behavior of polyethylene terephthalate. *Polymer* **2018**, *154*, 135−147.
(41) Hong, S.; Min, K.-D.; Nam, B.-U.; Park, O. O. High molecular weight bio furan-based co-polyesters for food packaging applications: Synthesis, characterization and solid-state polymerization. *Green Chem.* **2016**, *18*, 5142−5150.
(42) Flores, I.; Etxeberria, A.; Irusta, L.; Calafel, I.; Vega, J. F.; Martínez-Salazar, J.; Sardon, H.; Muller, A. PET-ran-PLA partially degradable random copolymers prepared by organocatalysis: effect of poly (l-lactic acid) incorporation on crystallization and morphology. *ACS Sustainable Chem. Eng.* **2019**, *7*, 8647−8659.
(43) Strobl, G.; Schneider, M.; Voigt-Martin, I. Model of partial crystallization and melting derived from small-angle X-ray scattering and electron microscopic studies on low-density polyethylene. *J. Polym. Sci., Polym. Phys. Ed.* **1980**, *18*, 1361−1381.
(44) Goderis, B.; Reynaers, H.; Koch, M.; Mathot, V. Use of SAXS and linear correlation functions for the determination of the crystallinity and morphology of semi-crystalline polymers. Application to linear polyethylene. *J. Polym. Sci., Part B: Polym. Phys.* **1999**, *37*, 1715−1738.
(45) Lu, X.; Hay, J. Isothermal crystallization kinetics and melting behaviour of poly (ethylene terephthalate). *Polymer* **2001**, *42*, 9423−9431.
(46) Hiemenz, P. C.; Lodge, T. P. *Polymer Chemistry*; 2007.
(47) Carter, P.; Trettin, J. L.; Lee, T.-H.; Chalgren, N. L.; Forrester, M. J.; Shanks, B. H.; Tessonnier, J.-P.; Cochran, E. W. Bioenabled Platform to Access Polyamides with Built-In Target Properties. *J. Am. Chem. Soc.* **2022**, *144*, 9548−9553.
(48) Khosravi-Darani, K.; Bucci, D. Application of poly (hydroxyalkanoate) in food packaging: Improvements by nanotechnology. *Chemical and Biochemical Engineering Quarterly* **2015**, *29*, 275−285.
(49) Boyer, R. Dependence of mechanical properties on molecular motion in polymers. *Polym. Eng. Sci.* **1968**, *8*, 161−185.
(50) Robeson, L.; Faucher, J. Secondary loss transitions in antiplasticized polymers. *Journal of Polymer Science Part B: Polymer Letters* **1969**, *7*, 35−40.
(51) Light, R.; Seymour, R. Effect of sub-Tg relaxations on the gas transport properties of polyesters. *Polym. Eng. Sci.* **1982**, *22*, 857−864.
(52) Burgess, S. K.; Leisen, J. E.; Kraftschik, B. E.; Mubarak, C. R.; Kriegel, R. M.; Koros, W. J. Chain mobility, thermal, and mechanical properties of poly (ethylene furanoate) compared to poly (ethylene terephthalate). *Macromolecules* **2014**, *47*, 1383−1391.
(53) Polyakova, A.; Connor, D.; Collard, D.; Schiraldi, D.; Hiltner, A.; Baer, E. Oxygen-barrier properties of polyethylene terephthalate modified with a small amount of aromatic comonomer. *J. Polym. Sci., Part B: Polym. Phys.* **2001**, *39*, 1900−1910.
(54) Codou, A.; Moncel, M.; van Berkel, J. G.; Guigo, N.; Sbirrazzuoli, N. Glass transition dynamics and cooperativity length of poly (ethylene 2, 5-furandicarboxylate) compared to poly (ethylene terephthalate). *Phys. Chem. Chem. Phys.* **2016**, *18*, 16647−16658.
(55) Lillwitz, L. Production of dimethyl-2, 6-naphthalenedicarboxylate: precursor to polyethylene naphthalate. *Appl. Catal. A: General* **2001**, *221*, 337−358.
(56) Reimschuessel, H. K. Poly (ethylene terephthalate) formation. Mechanistic and kinetic aspects of direct esterification process. *Industrial & Engineering Chemistry Product Research and Development* **1980**, *19*, 117−125.
(57) Ilavsky, J.; Jemian, P. R. Irena: tool suite for modeling and analysis of small-angle scattering. *J. Appl. Crystallogr.* **2009**, *42*, 347−353.
(58) Wang, T.-p.; Kang, D.-Y. Highly selective mixed-matrix membranes with layered fillers for molecular separation. *J. Membr. Sci.* **2016**, *497*, 394−401.

https://doi.org/10.1021/acs.macromol.2c00777
Macromolecules 2022, 55, 7785−7797

(59) Wang, T.-p.; Kang, D.-Y. Predictions of effective diffusivity of mixed matrix membranes with tubular fillers. *J. Membr. Sci.* **2015**, *485*, 123−131.

https://doi.org/10.1021/acs.macromol.2c00777
Macromolecules 2022, 55, 7785−7797